The Use of Vertical Wind Shear versus Helicity in Interpreting Supercell Dynamics

MORRIS L. WEISMAN AND RICHARD ROTUNNO

National Center for Atmospheric Research, Boulder, Colorado*

(Manuscript received 2 February 1999, in final form 10 June 1999)

ABSTRACT

A series of idealized simulations of supercell storms are presented for environments representing straight through circular hodographs to clarify the character of the storm dynamics over the large spectrum of hodograph shapes commonly observed. The primary emphasis is on comparing and contrasting recent theories of supercell dynamics, based on updraft–shear interactions, storm-relative environmental helicity (SREH), and Beltrami-flow solutions, to help clarify the degree to which each theory can represent the essential storm dynamics. One of the particular questions being addressed is whether storm dynamics are significantly different for straight versus curved hodographs, which has become a point of some controversy over recent years.

In agreement with previous studies, the authors find that the physical processes that promote storm maintenance, rotation, and propagation are similar for all hodograph shapes employed, and are due primarily to nonlinear interactions between the updraft and the ambient shear, associated with the localized development of rotation on the storm's flank. Significant correlations between the updraft and vertical vorticity are also observed across the shear spectrum, and, in agreement with predictions of linear theories associated with SREH, this correlation increases for increasing hodograph curvature. However, storm steadiness and propagation must already be known or inferred for such concepts to be applied, thus limiting the applicability of this theory as a true predictor of storm properties. Tests of the applicability of Beltrami solutions also confirm reasonable agreement for purely circular hodographs, for which the analytical solutions are specifically designed. However, analysis of the model results indicates that the terms ignored for such solutions, representing the nonlinear effects associated with storm rotation, are more significant than those retained over most of the hodograph spectrum, which severely limits the general applicability of such analyses.

1. Introduction

Over the past several years, two apparently disparate approaches have evolved in an attempt to understand the dynamics of supercell storms, based on either the role of vertical wind shear or the concept of storm-relative environmental helicity (SREH). The vertical wind shear perspective emphasizes the process by which an updraft interacts with the ambient vertical wind shear to produce a quasi-steady, rotating storm (e.g., Rotunno and Klemp 1982, 1985). On the other hand, the helicity approach postulates the existence of a steady, propagating storm, and then considers what storm motions would lead to the generation of updraft rotation via the tilting of environmental streamwise vorticity (e.g., Davies-Jones 1984). Paramount to this discussion is whether a storm generates rotation by virtue of its propagation, or whether the propagation is, in fact, a result of the development of storm rotation. In actuality, the two perspectives have much overlap, but the lack of a side-by-side comparison has lead to much confusion, especially when interpreting the potential for supercell storms for straight- versus curved-hodograph environments.

In this paper, we reexamine the fundamental basis for these theories, through the analysis of a series of supercell simulations representing a range of hodograph shapes. Our goal is to clarify the basic dynamical nature of supercells in the various shear regimes and to establish more clearly the degree to which the two theories help us understand and predict the behavior of supercell convection. In regard to the latter, we will reconfirm the storm motion–updraft rotation relationships that are central to the helicity perspective, but will argue that the updraft–shear interaction theory still represents the most general and flexible approach for understanding the full spectrum of supercell storm behavior.

The concept of a convective storm structure distinct from the paradigm of an ordinary thunderstorm dates back to Byers and Braham (1949), who noted that certain severe, long-lived cells developing in strongly sheared environments exhibited a tendency to propagate across rather than along the direction of the wind in the

* The National Center for Atmospheric Research is sponsored by the National Science Foundation.

Corresponding author address: Morris L. Weisman, NCAR, P.O. Box 3000, Boulder, CO 80307-3000.
E-mail: weisman@ncar.ucar.edu

cloud-bearing layer. Browning (1964) proposed that such storms were composed of a unique configuration of intertwined, possibly rotating updrafts and downdrafts that allowed the storm to survive for long periods, and coined the term ''supercell'' to descibe them. The advent of Doppler radar in the early 1970s confirmed the earlier observational deductions that the updraft regions within such cells also exhibit strong rotation about a vertical axis (e.g., vertical vorticities of order 0.01 s^{-1}), thus helping to explain their propensity to produce tornadoes. In many cases, these supercells were observed to originate through a process of storm splitting (e.g., Fujita and Grandoso 1968; Achtemeier 1969; Bluestein and Sohl 1979), with the right-moving member exhibiting cyclonic updraft rotation and the left-moving member exhibiting anticyclonic updraft rotation.

Many observational and modeling studies since have clarified the relationship between storm longevity, propagation, and the environmental vertical wind shear (e.g., Maddox 1976; Fankhauser and Mohr 1977; Johns et al. 1993; Weisman and Klemp 1982, 1984, 1986) and it is now accepted that strong vertical wind shear [e.g., generally greater than 20–25 m s^{-1} of wind variation over the lowest 4–6 km above ground level (AGL), usually measured as the length of the hodograph over that depth] is a necessary ingredient for the development of such long-lived structures (although short-lived rotating storms and tornadoes can occur in weaker-shear regimes). In addition, we have learned that the curvature of the wind shear profile on a hodograph plot can affect supercell evolution as well, with symmetric splitting supercells favored for nearly unidirectional shear profiles, and preferred right- or left-moving cells favored for clockwise- or counterclockwise-turning shear profiles, respectively (e.g., Klemp and Wilhelmson 1978b; Schlesinger 1980; Rotunno and Klemp 1982; Klemp 1987). The climatological hodograph most frequently associated with supercell environments, however, exhibits clockwise curvature, especially at low levels, thereby favoring a rightward-moving, cyclonically rotating storm, as is most commonly observed (e.g., Fig. 1, adapted from Maddox 1976).

Since the observational characteristic that distinguishes supercell convection from other types of convection is the development of a quasi-steady rotating updraft that can propagate across the environmental vertical wind shear, the fundamental question one must ask to understand supercells is what physical processes lead to the development of these storm properties. Along these lines, Newton and Newton (1959) proposed a physical theory linking wind shear with cell regeneration through ''lifting'' pressure gradients on the cross-wind flank of an existing storm cell. Along a slightly different vein, Barnes (1970) demonstrated that the movement of a thunderstorm across the environmental wind shear allows for a systematic tilting of the wind shear–associated horizontal vorticity to the vertical that could explain thunderstorm rotation. However, a theory connecting the propagation to the rotation was not addressed.

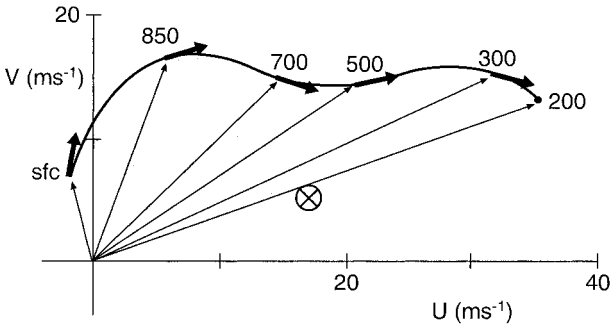

FIG. 1. Mean sounding (in m s^{-1}) for 62 tornado outbreak cases. The soundings are composited by computing the winds at each level relative to the estimated storm motion. Heavy arrows indicate the direction of the shear vector at each level (labeled in mb). The estimated mean storm motion is denoted by $\times$. The shaded region is proportional to the 0–3 km AGL storm-relative environmental helicity, as described by Davies-Jones (1984) (adapted from Maddox 1976).

The current arguments as to the role of vertical wind shear in controlling supercell dynamics represent an extension and refinement of the Newton and Newton (1959) hypothesis, and are largely based on the numerical and theoretical studies of Rotunno and Klemp (1982, 1985), as reviewed by Klemp (1987). The basic premise is that an updraft initially generates vertical vorticity at midlevels due to tilting of horizontal vorticity inherent in the ambient shear. This vertical vorticity then feeds back to the storm by contributing to dynamically induced pressure deficits that maximize at midlevels, producing nonhydrostatic vertical pressure gradients on the storm's flanks. It is these dynamically induced vertical pressure gradients that can force an updraft to propagate continuously toward a particular flank, thus allowing it to become well correlated with the vertical vorticity on that flank. Subsequently, this new updraft continues to tilt more horizontal vorticity on its flank, leading to a continuing process of updraft regeneration and propagation.

These physical processes are symmetric for unidirectional shear profiles (e.g., straight hodographs), leading to the generation of mirror-image ''splitting'' supercell storms, as are commonly observed for such environments, but are biased to the right- or left-moving storms for clockwise- or counterclockwise-curved shear profiles, respectively. Thus, from this perspective, the most basic paradigm for the dynamics of a supercell starts with the splitting process and is then modified to account for hodograph curvature.

The vorticity/helicity view of supercell dynamics is based on two somewhat independent concepts. The first has to do with the hypothesized tendency for helical structures within a turbulent flow to be more long lived than nonhelical flows, based on a reduced cascade of

energy to smaller scales. This idea was proposed for use in understanding the longevity of supercell storms by Lilly (1986b). The research on this hypothesis is still on going (e.g., Kanak and Lilly 1996), and will not be discussed further here.

The second concept, which is the one of primary interest here, is based on the use of streamwise and crosswise vorticity to characterize the rotational character of a quasi-steady propagating updraft (Rotunno 1981; Davies-Jones 1984; Lilly 1979, 1982, 1986a), similar to the approach of Barnes (1970). A study of the vertical vorticity equation linearized about an ambient vertically sheared environment shows that if an updraft propagates in the direction of the mean shear vector (i.e., on the hodograph), it will be characterized by a vortex couplet at midlevels, resulting in zero net updraft rotation. However, if the updraft propagates across the mean vertical wind shear vector (i.e., off the hodograph), it will exhibit a preferred sense of rotation; cyclonic if it moves to the right of the shear vector and anticyclonic if it moves to the left. Davies-Jones (1984) derived this correlation analytically, based on a linear analysis of the equations of motion. The measure of this predicted correlation is what has come to be known as storm-relative environmental helicity (SREH), which is proportional to twice the area bounded by the hodograph and by the storm-relative wind vectors, extending from the surface to some specified height above the surface [usually 3 km, AGL, as shown in Fig. 1; Davies-Jones et al. (1990)].

The concept of environmental streamwise vorticity is most easily visualized for a circular hodograph, where it is a reasonable assumption that storm motion resides near the center of the hodograph. In such a case, the environmental vorticity is purely streamwise at every height, leading to an apparently near-perfect correlation between the vertical velocity and the vertical vorticity. Furthermore, the full flow field can be approximated analytically by Beltrami-type solutions, which represent the limit of purely helical flow (e.g., the velocity vector and vorticity vector are parallel), and allows one to deduce certain relationships between the flow field and the pressure field within such a storm. Because of this ease in visualizing the impact of environmental streamwise vorticity and the possibility of analyzing the flow analytically, proponents of the helicity perspective view the circular-hodograph supercell as the most basic paradigm for interpreting supercell dynamics (e.g., Brooks and Wilhelmson 1993; Kanak and Lilly 1996).

While the concept of streamwise vorticity is generally straightforward, the assumptions that must be made to apply this concept to understanding supercell storms, namely, the existence of a quasi-steady updraft with known propagation characteristics, have lead to many misinterpretations concerning supercell dynamics in general. Straight-hodograph settings are especially problematic, as an anticipated mean storm motion on the hodograph leads to an apparent zero net updraft rotation, as the storm-relative flow has no streamwise component. Off-hodograph motion associated with the supercell dynamics must be assumed before the environmental storm-relative flow displays a streamwise component. Thus, the suggestion is often made that the dynamics of a straight-hodograph supercell is inherently different from that of a curved-hodograph supercell. This perspective is given theoretical support by suggesting that the development of updraft rotation for straight hodographs is inherently a nonlinear process, while it can be explained based on a linear analysis in a curved-hodograph setting (Davies-Jones 1984). However, Rotunno and Klemp (1982) suggest that nonlinear forcing is important to updraft maintenance and propagation for straight and curved hodographs alike, with the ''linear'' hodograph-curvature effects merely biasing a particular storm flank.

The questions we will readdress directly in this paper include the following: What is the essential dynamical character of supercell storms? Are the physical mechanisms responsible for the production of supercell storms inherently different for straight versus curved hodographs? Are these processes essentially linear or nonlinear? Does hodograph curvature lead to the development of a stronger, steadier, more rotational storm? To what degree do Beltrami solutions represent the dynamical character of supercells in the various shear regimes?

In the following, we will address these issues by reexamining a series of supercell simulations for purely straight through purely circular hodographs, to demonstrate the nature of the dynamic forcing producing the quasi-steady updraft structure for each case. In particular, we will show that the processes fundamental to the generation and maintenance of these updrafts are similar and are significantly nonlinear for all the hodograph shapes considered. This forcing is thus inconsistent with the conditions proposed for the helicity perspective, that the essential forcing within supercell storms is linear. Finally, by diagnosing the magnitudes of the terms in the full set of equations, we will also establish that the terms ignored in the Beltrami solutions are as significant as the terms retained, suggesting that Beltrami solutions do not capture the essence of supercell dynamics.

We will begin in section 2 with a description of the simulations being used in the present analysis. This will be followed in section 3 by an analysis of the storm dynamics, following the approach of Rotunno and Klemp (1982), to establish the linear versus nonlinear aspects of the solutions. Finally, in section 4, we will consider the degree to which these solutions can be represented by the simplified Beltrami model.

2. Overview of simulations

The simulations presented herein were completed using the Klemp and Wilhelmson (1978a) numerical cloud

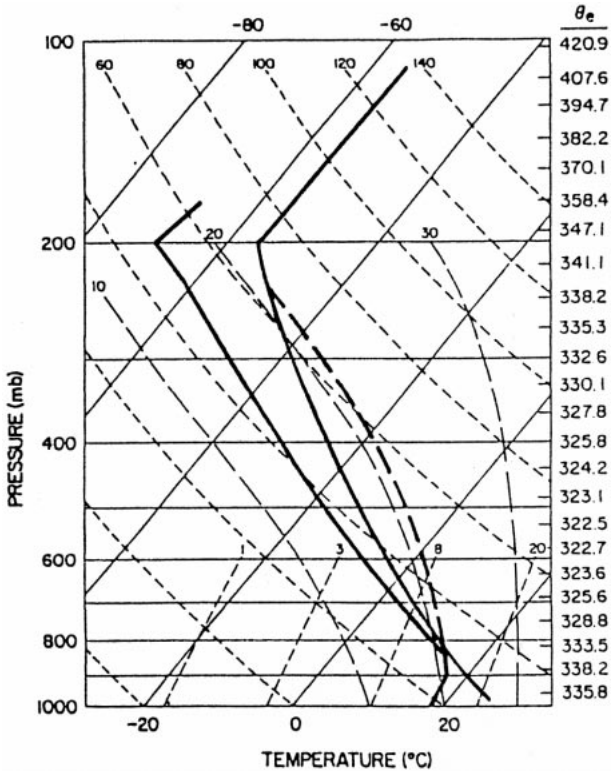

FIG. 2. Standard skew *T*–log*p* plot of initial temperature and moisture profile used in model simulations.

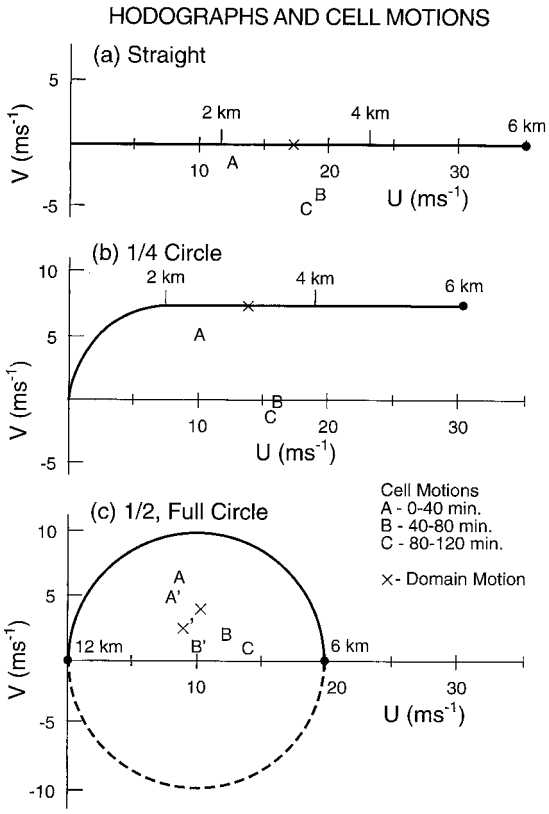

FIG. 3. Hodographs for the (a) straight shear, (b) quarter-circle shear, and (c) half- and full-circle shear profiles used for model simulations. Cell motions for each simulation are denoted by the symbols A, B, and C, representing average motions over the initial 40 min, 40–80 min, and 80–120 min, respectively. Winds remain constant above 6 km at the 6-km magnitude, except for the full-circle case, for which the shear extends up to 12 km, with the wind magnitude remaining constant above 12 km. The domain motion used in each simulation is depicted by the × with ×′ used for the full-circle simulation.

model, employing warm-rain Kessler microphysics, open lateral boundary conditions, a radiation-type boundary condition at the top of the domain (Klemp and Durran 1983), and a free-slip condition at the lower boundary. The grid spacing is 1 km in the horizontal and 500-m in the vertical. These resolutions are sufficient to resolve storm-scale features, such as the mid-level updraft structure and low-level mesocyclogenesis, but are not generally considered sufficient to accurately represent tornadogenesis. The domain is 120 km by 120 km by 17.5 km, with each simulation extending out through 2 h. Storms are triggered using an elipsoidal bubble of warm air of horizontal radius 10 km and vertical radius of 1400 m, with a maximum temperature perturbation of 1 K specified at the center of the bubble, decreasing to zero at its edges. Since Coriolis effects are minimal over a 2-h time period, the Coriolis parameter has been set to zero to simplify the interpretation of the results.

The thermodynamic profile used for each simulation (Fig. 2) is as used in Weisman and Klemp (1982, 1984, 1986), and represents an environment of moderate instability (2200 joules kg^{-1} of convective available potential energy, CAPE), with moist conditions throughout the troposphere. The vertical wind shear profiles for the base set of simulations (Fig. 3) are all characterized by 35 m s^{-1} of wind variation from the surface to 6 km AGL (e.g., the length of the hodograph, U_s, is 35 m s^{-1}), with the hodograph describing either a straight line (unidirectional shear profile), a quarter-circle shear profile to 2 km AGL with unidirectional shear above, or a half-circle shear profile through 6 km AGL. Winds are kept constant above 6 km. As previously presented in Weisman and Klemp (1982, 1984, 1986), a vertical wind shear magnitude of $U_s = 35$ m s^{-1} is well within the supercell regime for all three hodograph shapes employed. An additional simulation extends the shear layer for the half-circle hodograph case up to 12 km AGL, forming a complete circle, for a closer comparison with Beltrami-type solutions. A set of simulations was also completed for stronger-shear, $U_s = 45$ m s^{-1} environments but merely confirm the results presented herein. Weaker-shear simulations were also conducted, but produce less-steady storm structures, especially for the curved-hodograph cases.

An overview of the simulations is presented in Figs. 4, 5, and 6, which present a time series of the maximum vertical velocity and key aspects of the storm structure

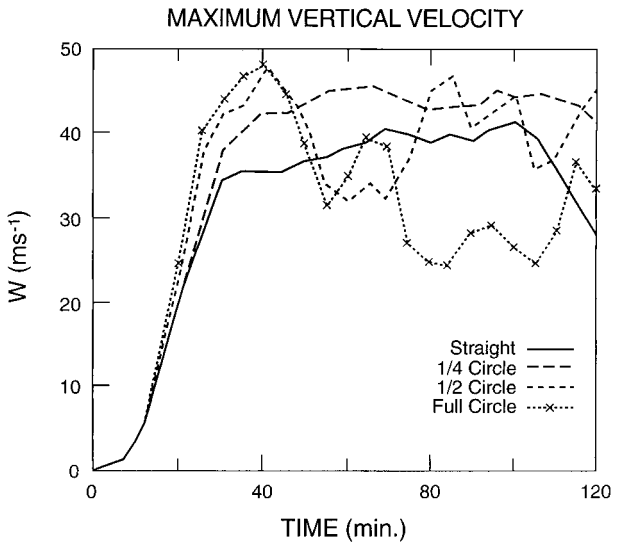

FIG. 4. Time series of maximum vertical velocity for the straight, quarter-circle, half-circle, and full-circle shear simulations.

at 3 km AGL at 40, 80, and 120 min for each case. All three storms evolve as previously described for supercell simulations, with the initial updraft impulse reaching its maximum strength by about 40 min, and then maintaining that strength in a quasi-steady fashion for the next 80 min. The full- and half-circle hodograph cases produce the strongest updrafts early on, but subsequently display significant unsteadiness through the remainder of the simulation. The supercell produced with the full-circle hodograph actually decays away completely by 60 min, being replaced by a system of shorter-lived ordinary cells triggered along the expanding outflow boundary to the northeast. The straight hodograph produces the weakest storm at early times but is comparable in strength to the other cases by 80 min. Overall, the quarter-circle hodograph case produces the strongest, most steady updraft of the cases considered.

The horizontal cross sections at 3 km AGL (Figs. 5 and 6) show a clear bias to the developing right-flank updraft by 40 min for increasing hodograph curvature, as described previously, with all four of these right-flank updrafts developing cyclonic rotation, and the left-flank updrafts being characterized by anticyclonic rotation. By 80 min, the right-flank cells for the straight-through-half-circle hodographs all display more mature supercell characteristics, with reflectivity hooks or notches on the southeast flanks of the storms, associated with the cyclonically rotating updrafts. The most ''classic'' looking supercell (e.g., Lemon and Doswell 1979), however, is produced in the quarter-circle hodograph case, with a pronounced hook on the southwest side of the cell and some suggestions of a V-notch configuration to the forward flank rain region. This case also produces the strongest low-level rotation, as is discussed further below. Left-flank cells continue to survive in all three cases, but are moving out the north boundary of the presented domain at this time. As noted above, the initial supercell for the full-circle hodograph has nearly decayed away by 80 min, being replaced by a line of ordinary cells to the northeast, along the spreading surface gust front. The storm configurations present at 80 min are generally maintained through 120 min, with some variation of updraft strengths and rainfield shapes evident during this period. Again, the most classic-looking supercell configuration is found with the quarter-circle hodograph case.

One of the attributes that characterizes supercell storms is that their motion deviates relative to the mean wind (and relative to nonsupercell storms). These propagational tendencies are closely tied to the development of rotation and the associated dynamic forcing of the updraft and, thus represent one of the key observational signatures that help identify a storm as being potentially supercellular. The cell motions for the four simulations are included on the hodographs (e.g., Fig. 3), with the motions presented for the 0–40-min, 40–80-min, and 80–120-min time periods. In all four cases, cell motions during the initial 40 min are generally in the direction of, but slower than, the mean wind over the lowest 6 km AGL. Between 40 and 80 min, however, all cases develop a significant propagational component to the right of the mean wind (and wind shear), consistent with the development of the rotational updraft after 40 min. (For the straight-hodograph case, the mirror-image left-moving cells are not included.) Cell motion then remains relatively constant between 80 and 120 min. Cell motion for the fully circular hodograph is not included between 80 and 120 min as the cell does not survive past 80 min. Thus, all four cases display a similar evolution of cell motion as the storms develop supercell characteristics.

Figure 7 presents time series of the maximum vertical vorticity associated with each supercell at 0.25 km and 3 km AGL. As previously described (e.g., Klemp 1987), vertical vorticity at midlevels in supercell storms is initially generated in the form of a vortex couplet centered on the updraft, as the updraft tilts the horizontal vorticity associated with the mean vertical wind shear. Over time, however, the updraft becomes more strongly correlated with one or both of these rotational centers (depending on hodograph curvature), leading to the development of a rotational storm. The timing of development and strength of this midlevel vertical vorticity is similar among all of the shear cases presented. The generation of significant vertical vorticity near the surface, however, is delayed to after 40 min, as near-surface vorticity production is critically dependent on the development of low-level downdrafts and the baroclinic generation of horizontal vorticity within the surface cold pool (e.g., Rotunno and Klemp 1985; Davies-Jones and Brooks 1993). The addition of hodograph curvature quickens the development of the near-surface vorticity a bit, but the strongest low-level vorticity occurs for the case with low-level curvature alone.

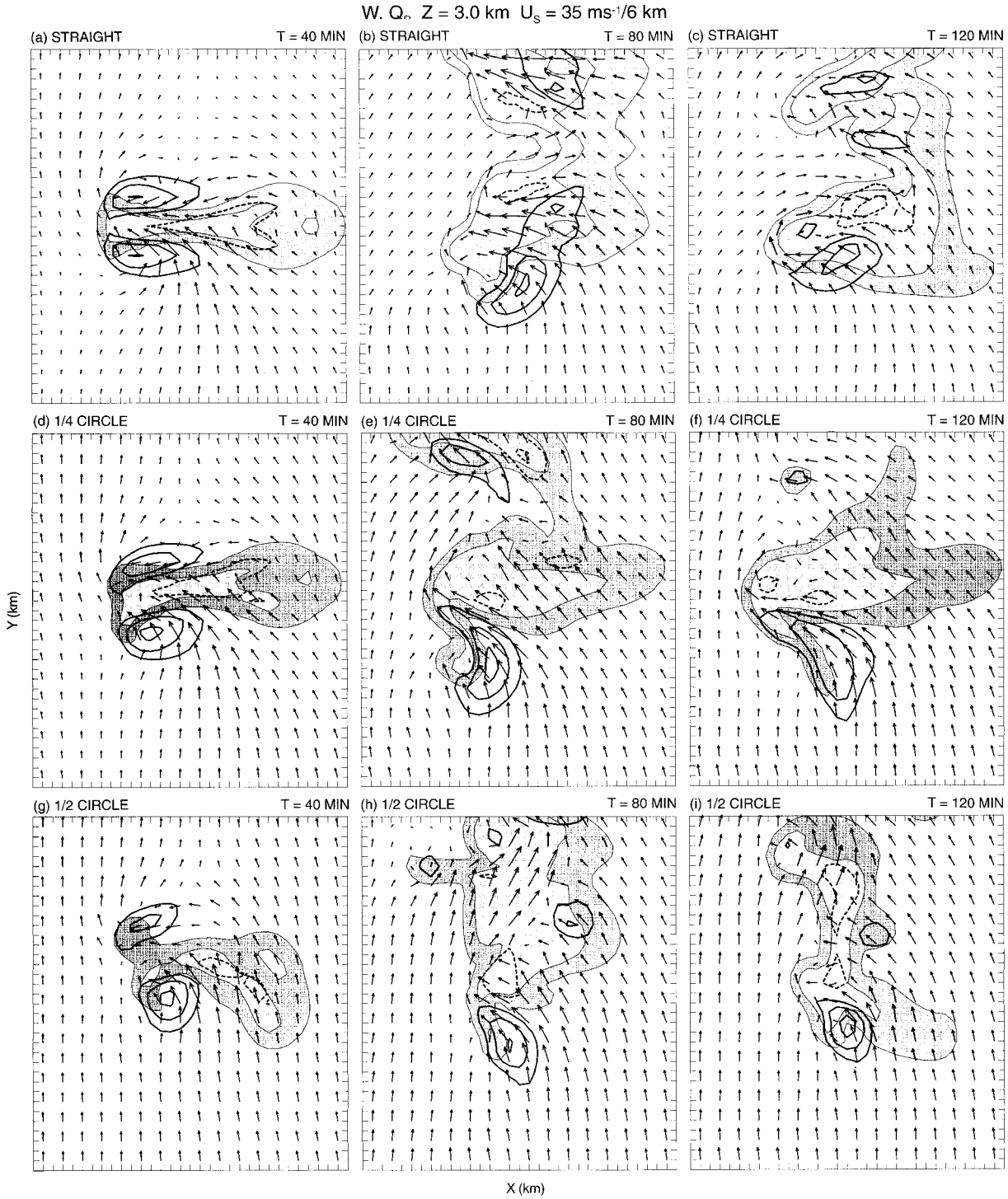

FIG. 5. Overview of storm structure at 40, 80, and 120 min at 3 km AGL for the (a), (b), (c) straight shear, (d), (e), (f) quarter-circle shear, and (g), (h), (i) half-circle shear simulations, respectively. The rainfield is shaded, with the dark shading representing rainwater mixing ratios of between 1 and 4 g kg^{-1}, and the lighter shading representing rainwater mixing ratios greater than 4 g kg^{-1}. The updrafts are contoured at 6 m s^{-1} intervals, with the zero contour ommitted. Vectors are drawn approximately relative to the cyclonic right-moving cell and are presented at every other grid point (2 km), with a vector length of one grid point equivalent to a vector magnitude of 10 m s^{-1}. The full domain has been windowed to a 32 km by 36 km region, centered on the moving storms.

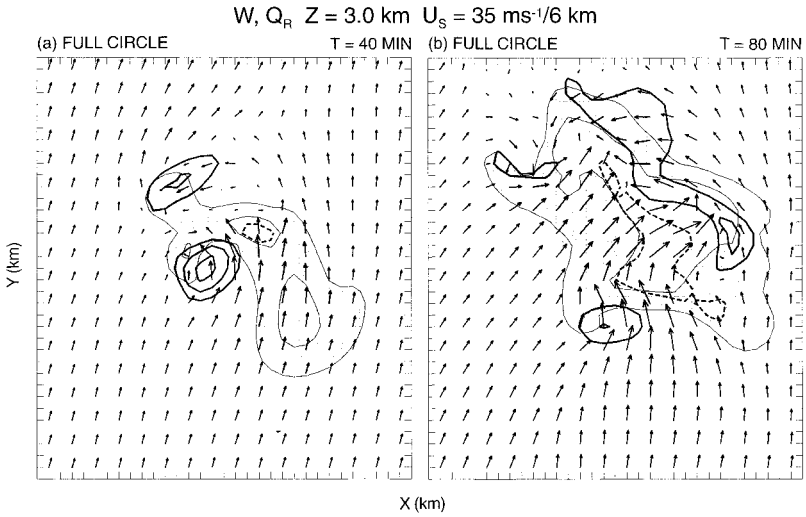

FIG. 6. Overview of storm structure at (a) 40 and (b) 80 min at 3 km AGL for the full-circle shear simulation, as described for Fig. 5.

The degree of correlation between the updraft and vertical vorticity has often been used as a measure of the significance of supercell processes within a given storm. Weisman and Klemp (1984) found mean correlations of between 0.5 and 0.8 over the lowest 8 km AGL for supercellular updrafts evolving in half-circle hodographs. Droegemeier et al. (1993) found similar magnitudes of updraft–vorticity correlation for supercells simulated for hodographs ranging from quarter-circle through three-quarter-circle shear cases, with the quarter-circle shear producing slightly lower correlations than the more strongly curved-hodograph cases. McCaul and Weisman (1996) calculated similar magnitudes for supercells evolving in hurricane landfall environments, also associated with strongly curved hodographs.

The development of significant updraft–vorticity correlations for the present cases is apparent from Fig. 8, which presents an overlay of the vertical velocity and vertical vorticity fields at 3 km AGL at 40 min. The magnitude of the linear correlation coefficient (Panofsky and Brier 1968) through the depth of each storm is presented in Fig. 9 at 40, 80, and 120 min. These calculations were made within an approximate 15 km by 15 km box surrounding the particular updraft cell, and only included points where the vertical velocity was greater than 1 m s^{-1}. By 40 min, correlations of 0.5 or greater have already been established at midlevels for both the straight and quarter-circle shear simulations, with correlations of 0.5 or greater also evident, but at lower elevations, for the half-circle and full-circle hodographs. By 80 min, the correlations for the half-circle case have increased to between 0.6 and 0.8 over the lowest 10 km of the updraft, with the correlations maintaining between 0.4 and 0.6 for the quarter-circle case, and dropping to between 0.2 and 0.4 for the straight-hodograph case (the full-circle storm has disipated by this time). By 120 min, the half-circle correlations have decreased somewhat, with the quarter-circle shear case now displaying the largest correlations. Thus, while there is a tendency for the storms to develop larger updraft–vorticity correlations for increasing hodograph curvature, the larger curvature cases do not necessarily produce the most consistent correlations, due largely to the more unsteady nature of these storms.

The degree of storm unsteadiness noted for the more curved-hodograph environments could result both from the increased tendency for the rain to fall back into the main updrafts as well as the increased tendency for the surface cold pool to propagate away from the storm. In order to test the sensitivity of these simulations to the strength of the rainfall and surface outflow, we also completed a set of simulations for the four hodograph types in which the rain processes were eliminated, with the condensate instead remaining in the form of cloud water (which advects with the airflow). Without rainfall and rain evaporation at mid- and low levels, there is no low-level cooling, and a surface cold pool fails to form. These no-rain simulations could, thus, be considered an extreme end of such rainfall–outflow sensitivity experiments.

As before, supercells form in all four cases, with symmetric splitting evident in the unidirectional shear case and the cyclonic, right mover becoming more prevalent as hodograph curvature is added (not shown). Thus, as also discussed by Rotunno and Klemp (1985), rainfall and cold pools are not necessary for the production of these long-lived rotating storms. The relative strengths and kinematical features of the various cases also remained the same, with the quarter-circle case still producing the strongest and steadiest rotating updraft. However, the storms produced in the half-circle and full-circle cases are now nearly as steady as for the straighter-shear cases, confirming that inherent updraft

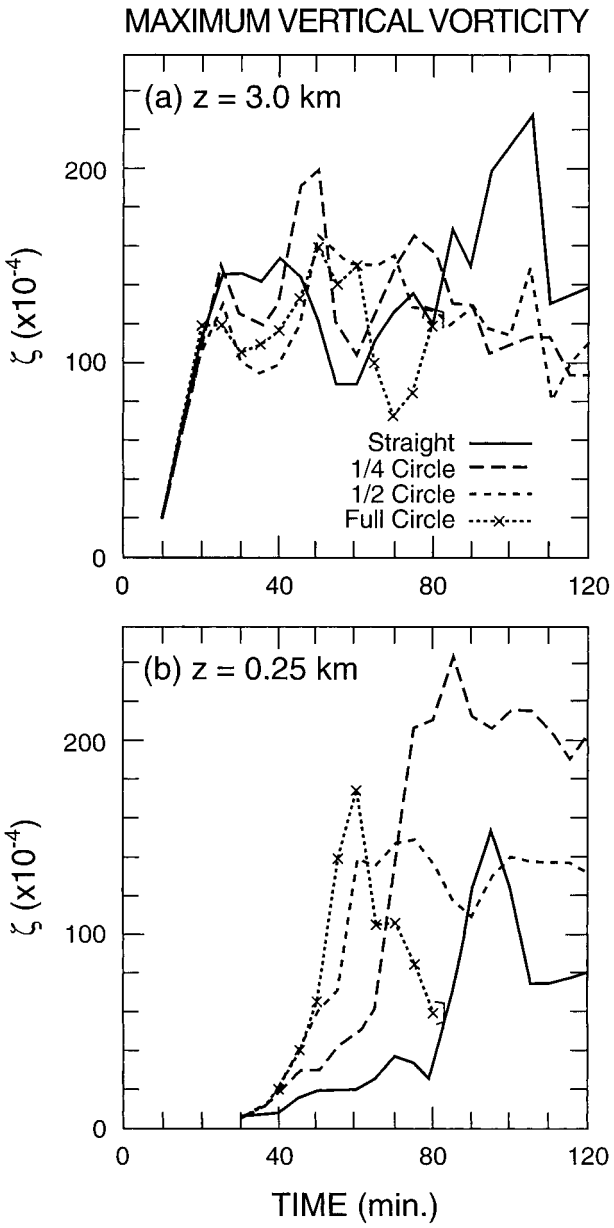

FIG. 7. Time series of maximum vertical vorticity (10^4 s^{-1} for the straight, quarter-circle, half-circle, and full-circle shear simulations at (a) 3 km AGL and (b) 0.25 km AGL.

steadiness can be linked to microphysical and dynamical processes alike. Further discussion of such microphysical sensitivities, however, is beyond the scope of the present paper.

In summary, all four shear profiles produce storms that develop significant supercellular features over a similar time frame and via a similar sequence of events. The kinematic structure of the various storms varies somewhat over the hodograph types, with the cyclonic right-moving updraft becoming more dominant and more strongly correlated with positive vertical vorticity as more hodograph curvature is added. However, increasing the hodograph curvature to a full circle fails to produce a long-lived storm for the standard warm-rain microphysics employed. In the next section, we investigate the degree of significance of the kinematical differences among the four full-rain simulations through a more detailed analysis of the dynamics of each storm. Similar analyses were also completed for the no-rain cases but merely confirm the basic relationships established for the full-rain simulations.

3. Theoretical arguments

Historically, the attempts to understand the dynamics of supercell storms have encompassed a wide range of methodologies, from detailed analyses of the full equations of motion, to the application of much more simplified models that attempt to capture the essence of the storm dynamics. The ultimate goal is to find a general analytical solution that explains not only storm maintenance and propagation, but also storm evolution for the full range of observed supercell environments. Achieving this goal is made exceptionally difficult by the highly nonlinear, time-dependent nature of the governing equations. Thus, many researchers have investigated simplified forms of the equations, considering, for instance, steady solutions in which the nonlinear properties are more easily addressed (e.g., Beltrami solutions), or linearized versions of the equations with the hope that they contain the essential dynamics (e.g., the streamwise vorticity/helicity approach). The apparent steadiness of supercell storms offers hope that such approaches could shed some light on the dynamics. However, neither of these approaches can address issues relevant to storm evolution. Another approach taken has been to analyze the full set of nonlinear time-dependent equations in the hope of identifying a chain of diagnostic relations that close the loop on storm evolution, maintenenance, and propagation. This has been the approach taken when applying the wind shear arguments.

In the following, we will review the assumptions and conclusions that are associated with each methodology, in hopes of clarifying the basic dynamics of supercell storms. We will begin with the most general approach, which is based on diagnostics from the full time-dependent equations, followed by a discussion of the more simplified approaches, which assume steady-state conditions and/or linearizations of the basic equations.

a. Updraft–vertical wind shear interactions

The basic equation set that is generally used to interpret supercell dynamics is the inviscid, Boussinesq equations of motion,

$$\frac{\partial \mathbf{v}}{\partial t} + \mathbf{v} \cdot \nabla \mathbf{v} = -C_p \overline{\theta}_v \nabla \pi + B\mathbf{k}, \qquad (1)$$

where B is the full buoyancy, given by

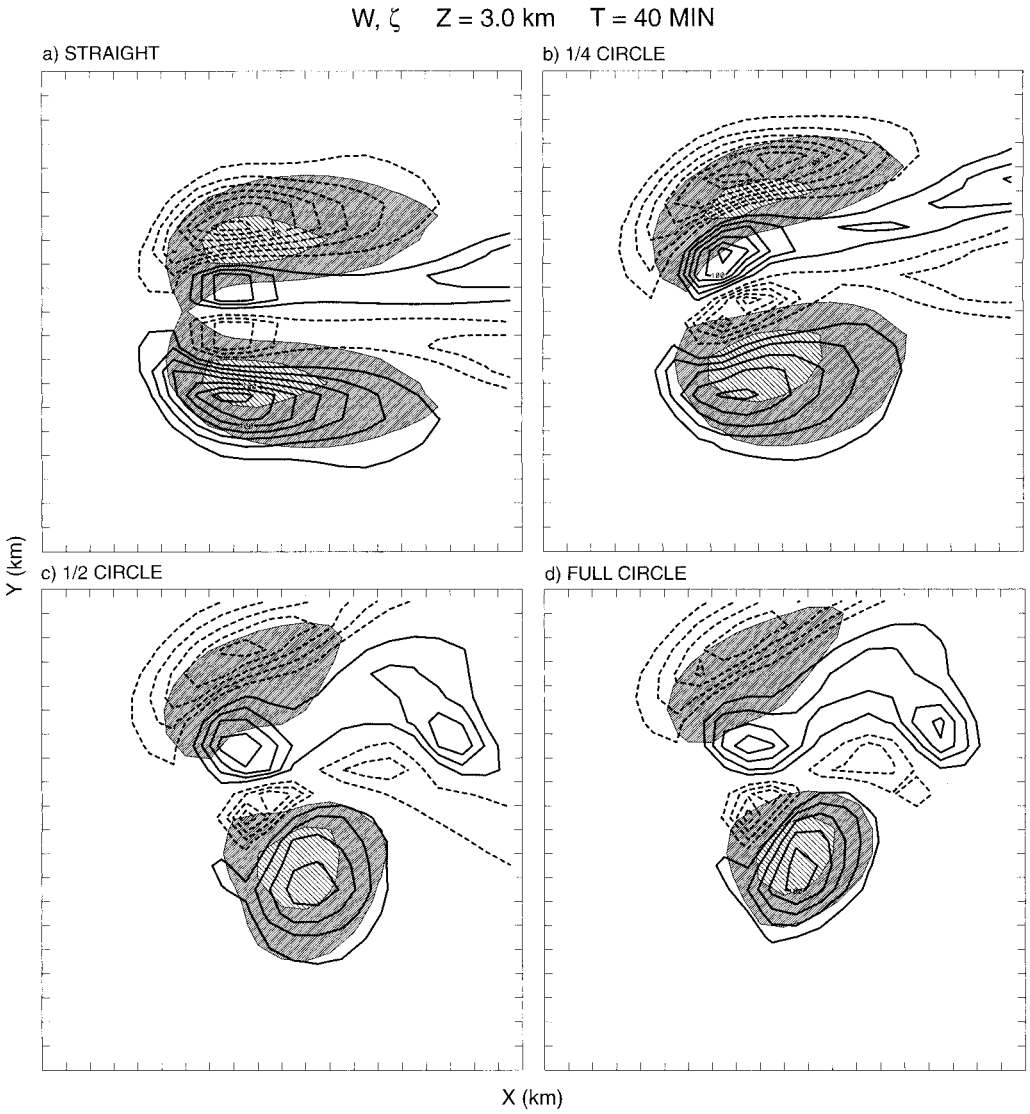

FIG. 8. Vertical vorticity and vertical velocity at 3 km AGL at 40 min for the (a) straight shear, (b) quarter-circle shear, (c) half-circle shear, and (d) full-circle shear simulations. The updraft region is cross hatched, with the dark and light hatching representing vertical velocities between 4 and 14 m s^{-1}, and greater than 14 m s^{-1}, respectively. Vertical vorticity is contoured at 0.002 s^{-1} intervals, with the zero contour omitted. The full domain has been windowed to a 20 km by 20 km region, centered on the moving storms. Tick marks are included every km.

$$B \equiv g\left[\frac{\theta'}{\overline{\theta}} + 0.61(q_v - \overline{q}_v) - q_c - q_r\right], \qquad (2)$$

and π is the Exner function, given by

$$\pi \equiv \left(\frac{p}{p_0}\right)^{R_d/C_p}. \qquad (3)$$

Supercell storms are most clearly distinguished from ordinary convection by their tendency to develop a quasi-steady updraft that propagates across the environmental vertical wind shear. Thus, to understand the dynamics of such storms, we are especially interested in characterizing the nature of the updraft forcing that produces such a sustained, propagating storm,

$$\frac{dw}{dt} = -C_p\overline{\theta}_v\frac{\partial\pi}{\partial z} + B. \qquad (4)$$

We are also interested in how such updrafts develop rotation about a vertical axis, and so we present the vertical vorticity equation,

$$\frac{d\zeta}{dt} = \boldsymbol{\omega}_H \cdot \boldsymbol{\nabla}_H w + \zeta\frac{\partial w}{\partial z}. \qquad (5)$$

Rotunno and Klemp (1982) and Weisman and Klemp (1984) suggest that the essential dynamics that distin-

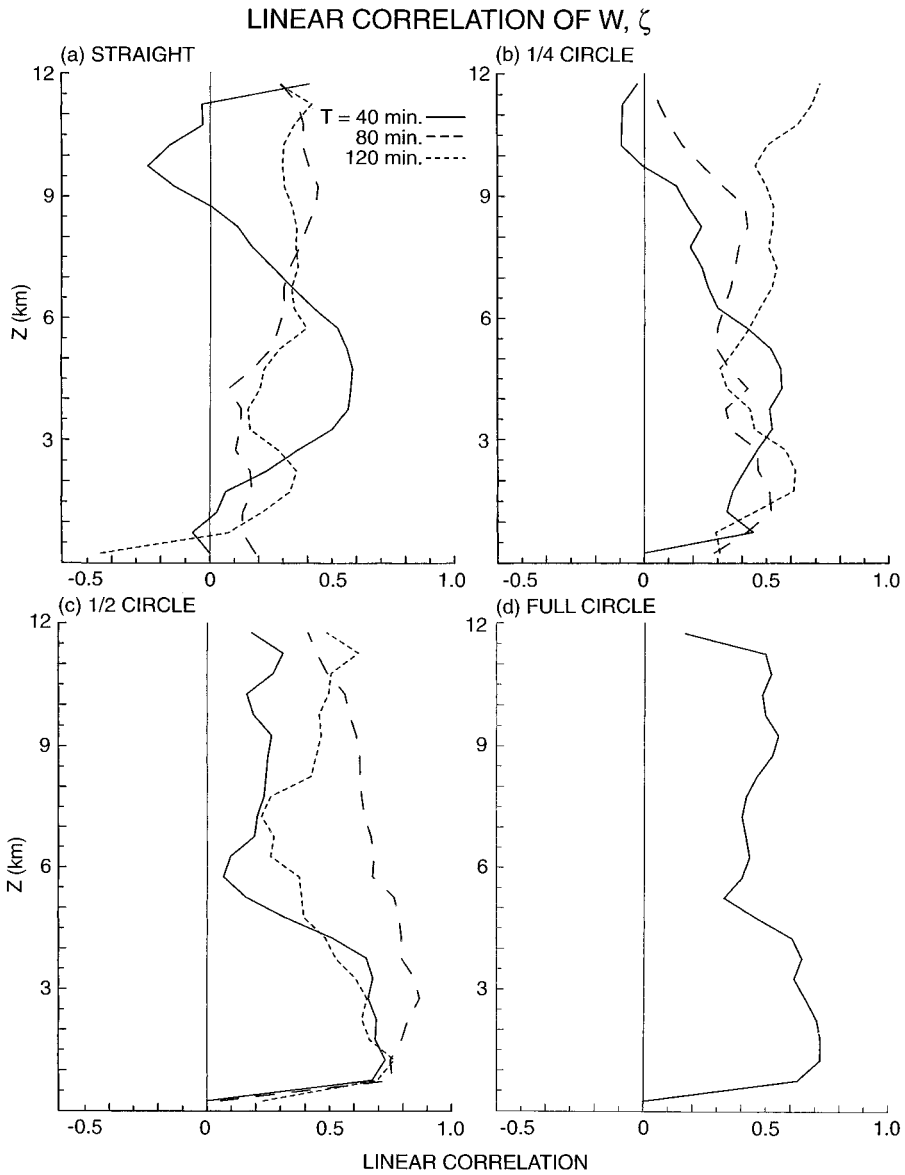

FIG. 9. Linear correlation of vertical vorticity and vertical velocity at 40, 80, and 120 min for the (a) straight shear, (b) quarter-circle shear, (c) half-circle shear, and (d) full-circle shear simulations. Correlations for the full-circle simulations are presented only at 40 min, as the storm dissipates before 80 min.

guish supercellular updrafts from ordinary convective updrafts that develop in weaker-shear regimes is largely encompased in the vertical pressure gradient term. The nature of this vertical pressure gradient forcing is clarified via a diagnostic pressure equation, which is derived by taking the divergence of the three-dimensional momentum equation (1) and using the anelastic-continuity equation, $\nabla \cdot (\overline{\rho}\mathbf{v}) = 0$:

$$\nabla \cdot (C_p \overline{\rho}\, \overline{\theta}_v \nabla \pi) = -\nabla \cdot (\overline{\rho}\mathbf{v} \cdot \nabla \mathbf{v}) + \frac{\partial \overline{\rho} B}{\partial z}. \quad (6)$$

The contributions to the pressure perturbations can then be divided into those associated with variations in the velocity field, π_{dn}, and those associated with the buoyancy field, π_B, by solving the two Poisson equations:

$$\begin{aligned} \nabla \cdot (C_p \overline{\rho}\, \overline{\theta}_v \nabla \pi_{dn}) &= -\nabla \cdot (\overline{\rho}\mathbf{v} \cdot \nabla \mathbf{v}) \\ &= -2\overline{\rho}\left[\frac{\partial v}{\partial x}\frac{\partial u}{\partial y} + \frac{\partial u}{\partial z}\frac{\partial w}{\partial x} + \frac{\partial v}{\partial z}\frac{\partial w}{\partial y}\right] \\ &\quad - \overline{\rho}\left[\left(\frac{\partial u}{\partial x}\right)^2 + \left(\frac{\partial v}{\partial y}\right)^2 + \left(\frac{\partial w}{\partial z}\right)^2 - \frac{d^2 \ln \overline{\rho}}{dz^2} w^2\right] \quad (7) \end{aligned}$$

and

$$\nabla \cdot (C_p \overline{\rho}\, \overline{\theta}_v \nabla \pi_B) = \frac{\partial(\overline{\rho} B)}{\partial z}, \quad (8)$$

subject to the boundary conditions $\partial \pi_{\rm dn}/\partial z = 0$ and $\partial \pi_B/\partial z = B$ on $z = 0, h$, where $\pi = \pi_{\rm dn} + \pi_B$. The vertical momentum equation can then be written to reflect the dynamic and buoyancy contributions to the vertical acceleration;

$$\frac{dw}{dt} = -C_p \overline{\theta}_v \frac{\partial \pi_{\rm dn}}{\partial z} + \left[-C_p \overline{\theta}_v \frac{\partial \pi_B}{\partial z} + B \right]. \quad (9)$$

Based on analyses of the rhs of (9) for simulated supercell storms, Rotunno and Klemp (1982) and Weisman and Klemp (1984) showed that the unique strength, steadiness, and propagational characteristics of supercell storms is directly attributable to the strength and configuration of the dynamic pressure gradient term, which continually forces updraft growth on the flank of the original updraft. This dynamic forcing is symmetric about the shear vector for unidirectional shear profiles (straight hodographs), producing symmetric splitting in such environments, but is biased to the right or left flank of the updraft for clockwise- or counterclockwise-curved hodographs, leading to preferred cyclonic right-moving or anticyclonic left-moving supercells, respectively.

Furthermore, Rotunno and Klemp (1985) have shown that it is the contributions to the pressure from the first bracketed term on the rhs of (7), representing contributions from fluid shear, that produce the forcing on the flank of the updraft that is critical for storm propagation. Since these fluid shear terms contribute to negative pressure perturbations, this dynamical forcing can then be directly related to the development of local rotation on the flanks of the storm (both horizontal and vertical), thereby directly connecting the rotational nature of supercell updrafts to their maintenance and propagation. The terms in the second bracket on the rhs of (7) represent contributions to pressure field from fluid extension, are generally collocated with the updraft, and thus do not contribute to updraft propagation.

The dynamic pressure contributions can be further decomposed into linear, $\pi_{\rm L}$, and nonlinear, $\pi_{\rm NL}$, contributions, where $\pi_{\rm L}$ is determined by only considering the contributions to the dynamic pressure from terms involving the ambient vertical wind shear,

$$\nabla \cdot (C_p \overline{\rho}\, \overline{\theta}_v \nabla \pi_{\rm L}) = -2\overline{\rho} \left[\frac{\partial U}{\partial z} \frac{\partial w}{\partial x} + \frac{\partial V}{\partial z} \frac{\partial w}{\partial y} \right], \quad (10)$$

where $U(z)$ and $V(z)$ represent the ambient wind profile. Here $\pi_{\rm NL}$ is calculated using (7) after subtracting the linear contributions given by the rhs of (10). Rotunno and Klemp (1982) demonstrated that it is the linear contributions that provide the forcing bias for curved versus straight hodographs, producing a preferred cyclonic right-moving supercell for clockwise-curved hodographs and a preferred anticyclonic left-moving supercell for counterclockwise-curved hodographs. However, the nonlinear contribution to the forcing and propagation was still found to be dominant for both straight and curved hodographs.

In order to again demonstrate the relative importance of the various forcing terms in controlling supercell dynamics, we have diagnosed the dynamic, linear, and nonlinear contributions to the vertical accelerations for the four simulations described in section 2, representing straight, quarter-, half-, and full-circle hodograph settings. By applying this analysis to the full model solutions, we extend the results of Rotunno and Klemp (1982), which considered only the early evolution of an updraft in a sheared flow using the shallow, inviscid, and anelastic equations (Ogura and Phillips 1962). Analyses are presented at both 40 and 80 min into each simulation, to represent the character of the forcing for both the early and mature phase of each supercell. We will present the dynamic forcing at 3 km AGL as representative of the primary updraft forcing for each case.

At 40 min (Fig. 10), the dynamic forcing for the unidirectional-shear case is characterized by symmetric areas of positive forcing on the flanks of the initial cell, associated with a developing cyclonic, right-flank and anticyclonic left-flank updraft, as is characteristic of the early stages of splitting supercells. A decomposition of the forcing into linear and nonlinear components reveals that the splitting process is dominantly nonlinear, with only very weak linear contributions on the downshear flank of the cell, similar to Rotunno and Klemp (1982, Fig. 8). As low-level curvature is added to the wind shear profile, the dynamic forcing becomes slightly biased to the right flank of the storm, favoring the cyclonic member of the splitting pair. The bias is directly attributable to a bias in the linear forcing, but the nonlinear terms are clearly still dominant. For the half-circle hodograph, the right-flank bias is more significant yet, but the nonlinear forcing is still significantly stronger than the linear forcing. Finally, for the circular hodograph (Fig. 11), the linear and nonlinear forcing are more comparable, but the nonlinear forcing still dominates.

At 80 min (Fig. 12), once the supercells have developed a mature structure, the nonlinear forcing is still dominant, even for the half-circle shear case, emphasizing the truly nonlinear character of these types of storms. Interestingly, the largest linear contribution to the forcing at this time is found with the unidirectional shear case. The enhanced linear forcing in this case seems related to the elongation and reconfiguration of the upraft region from an east–west to a north–south orientation. The full-circle shear storm has decayed by this time and is, thus, not presented.

In order to more clearly document the contributions to updraft forcing for the various simulations, time-dependent updraft trajectories were calculated in which the dynamic, linear, and nonlinear pressure forcing terms were interpolated along the parcel's path. These trajectories were calculated using model data saved at

a 5-min time interval, using a 250-m interpolation interval along the parcel's path. As in Weisman and Klemp (1984), the forcing terms are then integrated over time to represent their net contribution to updraft strength along the trajectory,

$$w(x, y, z, t) = w_0 + \int_T -C_p \overline{\theta}_v \frac{\partial \pi_{dn}}{\partial z}\, dt + \int_T \left[-C_p \overline{\theta}_v \frac{\partial \pi_b}{\partial z} + B \right] dt. \quad (11)$$

The observed vertical velocities were also interpolated along the trajectories for comparison with the integrated forcing terms. We find that the diagnosed vertical velocities matched the observed vertical velocities within about 10% up to the level of maximum vertical velocity, but the accuracy decreases above this level due to the accumulated effects of mixing. Such trajectories and updraft forcing analyses were constructed for the entire updraft region for each simulation, at both 40 and 80 min, but results will be shown only for the trajectories going through the maximum updraft at 3 km AGL, as these trajectories were found to be generally representative of the overall character of the updrafts for each case. The average time integration period, T, for each trajectory was 20 min, both forward and backward from the starting point at 3 km AGL.

By 40 min, the right-flank updrafts have all begun to develop supercellular characteristics, with the updrafts becoming positively correlated with cyclonic rotation (e.g., Fig. 8). As shown in Fig. 13, the total dynamic contributions to updraft strength range between 40% and 60% of the observed maximum updraft magnitudes along the trajectories. This is consistent with the findings of Weisman and Klemp (1984) and McCaul and Weisman (1996), who show similar magnitudes of dynamic forcing associated with supercellular updrafts. Of particular significance is the strong dynamic forcing found through the lowest several kilometers of the storm, which is often much greater in magnitude than the contributions from buoyancy at those levels. The integrated contributions from the linear forcing terms are negligible for both the unidirectional and quarter-circle shear cases, but do contribute 20%–30% of the dynamic forcing for the half-circle and full-circle cases.

By 80 min (Fig. 14), the dynamic contributions to updraft strength still range between 50% and 60%, with the nonlinear contributions still clearly dominating for both the quarter- and half-circle shear cases, and, interestingly, the linear and nonlinear contributions more nearly equal in the unidirectional shear case. The overall message of this analysis, though, is that the nonlinear contributions to updraft forcing are generally dominant, independent of hodograph curvature, and these nonlinear effects must be considered in explaining or predicting supercell behavior for both straight and curved hodographs.

The full relationship between storm maintenance, propagation, and rotation for the present simulations is summarized in Fig. 15, which displays the phase relationship between the flow field, vertical vorticity, dynamic pressure gradient forcing, and tilting (in vertical cross sections through the center of the updrafts) for the cyclonic right-moving storms for the straight- and half-circle hodograph cases at 40 min. From the vertical wind shear perspective, it is the localized development of rotation on the flanks of the initial updraft, produced via the tilting (and subsequent stretching) of vortex lines associated with the strong, ambient vertical wind shear, that leads to the development of a significant dynamic vertical pressure gradient force on the updraft flank. This dynamic forcing, which is significantly nonlinear for all hodograph shapes employed, forces the updraft to propagate to the right (as in Fig. 15), subsequently leading to the development of a correlation between the updraft and the midlevel rotation. The further generation of rotation on the flanks of the updraft via tilting then continues to promote the maintenance and propagation of the updraft in this new configuration.

b. Quasi-linear approaches

The advantage of the vertical wind shear approach is that the forcing for the supercell is derived in a completely general manner, without any assumptions concerning the steadiness or propagational characteristics of the given storm. However, the complexities of this full system of equations has thus far precluded the development of an analytic solution, thus limiting our ability to develop a more concise theory for the evolution of such storms. It has been the attempt to develop an appropriate simpler theory that has motivated many of the other efforts to understand supercell dynamics.

Although it is well recognized that convective storms are highly nonlinear phenomena, many of the simplified approaches have used a selective linearization of the basic equations (e.g., some nonlinear terms such as the vertical advection of buoyancy are kept implicitly) in an attempt to understand specific characteristics of the storm dynamics, such as rotation and propagation. Of particular importance to the present discussion, the linearized form of the diagnostic pressure equation (6) becomes

$$\nabla \cdot (C_p \overline{\rho}\, \overline{\theta}_v \nabla \pi) = -2\overline{\rho} \left[\frac{\partial U}{\partial z} \frac{\partial w}{\partial x} + \frac{\partial V}{\partial z} \frac{\partial w}{\partial y} \right] + \frac{\partial (\overline{\rho} B)}{\partial z}, \quad (12)$$

and the vertical vorticity equation (5) becomes

$$\frac{\partial \zeta}{\partial t} + U \frac{\partial \zeta}{\partial x} + V \frac{\partial \zeta}{\partial y} = + \frac{\partial U}{\partial z} \frac{\partial w}{\partial y} - \frac{\partial V}{\partial z} \frac{\partial w}{\partial x}. \quad (13)$$

The primary difference physically between the full (6) and linearized (12) forms of the diagnostic pressure

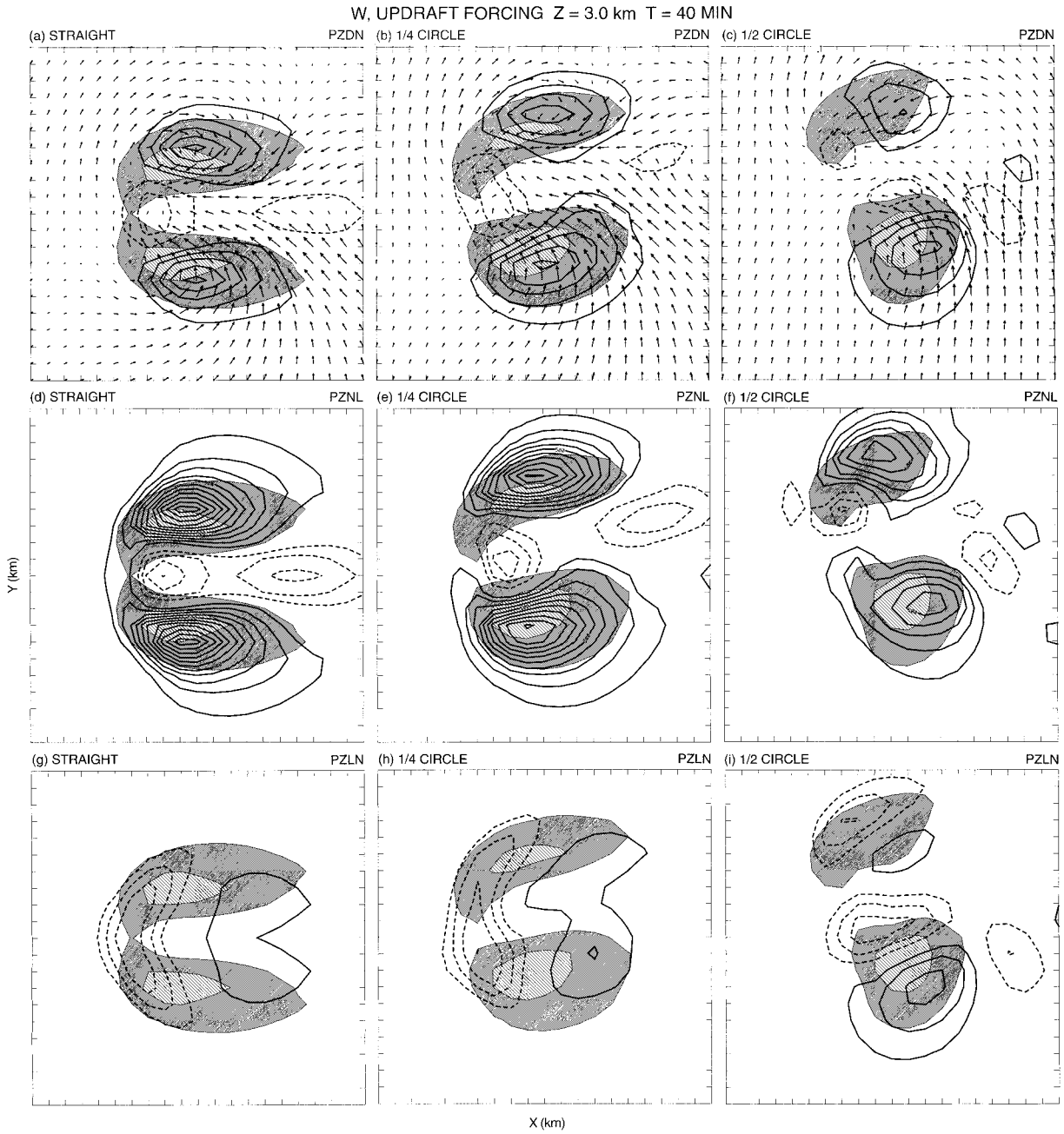

FIG. 10. Dynamic (PZDN), nonlinear (PZNL), and linear (PZLN) updraft forcing at 3 km AGL at 40 min for the (a), (d), (g) straight shear, (b), (e), (h) quarter-circle shear, and (c,f,i) half-circle shear simulations, respectively. PZDN is contoured at 0.002 m s^{-2} intervals, with PZNL and PZLN countoured at 0.001 m s^{-2} intervals, all with the zero contour omitted. The updraft region is cross hatched, with the dark and light hatching representing vertical velocities between 4 and 14 m s^{-1}, and greater than 14 m s^{-1}, respectively. (a), (b), (c) Vectors are drawn approximately relative to the cyclonic, right-moving cell and are presented at every grid point (1 km), with a vector length of one grid point equivalent to a vector magnitude of 20 m s^{-1}. The full domain has been windowed to a 20 km by 20 km region, centered on the moving storms. Tick marks are included every km.

equation is the absence of nonlinear contributions to the pressure perturbations from rotational effects (among others). The primary difference between the full (5) and linear (13) forms of the vertical vorticity equation is the absence of stretching and vertical advection. Thus, an important measure of the ability of the linearized equations (12) and (13) to explain supercell dynamics is the degree to which rotationally induced pressure perturbations and vortex stretching are critical components of those dynamics.

Rotunno and Klemp (1982) used (12) to deduce the pressure distribution for a given symmetrically shaped

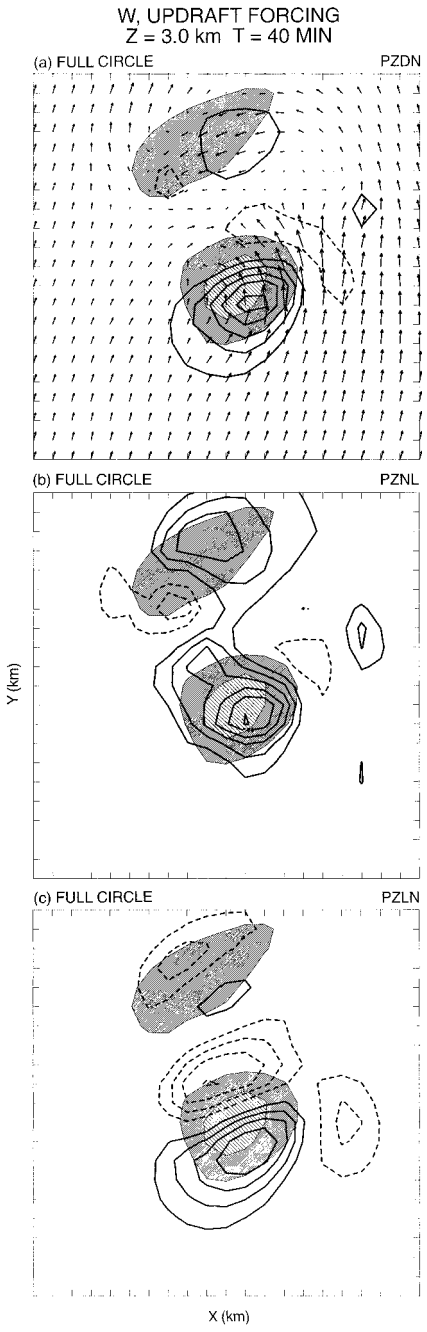

FIG. 11. (a) Dynamic (PZDN), (b) nonlinear (PZNL), and (c) linear (PZLN) updraft forcing at 3 km AGL at 40 min for the full-circle shear simulation, as described for Fig. 10.

updraft. Lilly (1979, 1982, 1986a), Rotunno (1981), and Davies-Jones (1984) used (13) to deduce the correlation between the vertical vorticity and the updraft, w, of a *given* size, shape, and propagational characteristics. For example, for a steady-inviscid updraft propagating transverse to a unidirectional environmental shear profile at a velocity of c_y, (13) becomes

$$-c_y \frac{\partial \zeta}{\partial y} = \frac{\partial U}{\partial z} \frac{\partial w}{\partial y}, \tag{14}$$

which can be integrated immediately to obtain (e.g., Lilly 1979)

$$\zeta = \frac{\partial U}{\partial z} \frac{w}{-c_y}. \tag{15}$$

Thus, a steady updraft propagating across the shear would be expected to be strongly correlated with the vertical vorticity field, as is confirmed from observations and modeling studies. Thus, *given* a steady propagating updraft, storm rotation can be deduced based simply on quasi-linear analysis. However, the question of what maintains the storm and forces the observed propagation is not addressed. (In other words, c_y and w are not necessarily the eigenvalues and eigenfunctions of the full linearized equations.)

Davies-Jones (1984) generalized the analysis leading to (15) to two-dimensional shear profiles and showed that the covariance of vertical velocity and vertical vorticity at a given level is proportional to the storm-relative environmental streamwise vorticity, $(\mathbf{v} - \mathbf{c}) \cdot \boldsymbol{\omega}$. The physical basis for this relationship is most easily visualized in Fig. 16 (from Davies-Jones 1984), which depicts the flow field for idealized steady-state updrafts (represented by a displacement peak or ''hump'' in the isentropic surface) for cases of purely crosswise or streamwise storm-relative environmental vorticity. For the crosswise case, storm-relative flow lifts the ambient vortex lines symmetrically about the updraft, producing a vortex couplet at midlevels centered on the updraft, with zero updraft–vorticity correlation. For the streamwise case, the storm-relative flow is oriented along the vortex lines, and the updraft and vertical vorticity are strongly correlated. The fact that the vortex lines remain in their original isentropic surfaces as the surfaces are deformed by the storm is a direct statement of the conservation of equivalent potential vorticity (Ertel's theorem), as discussed by Davies-Jones (1984) and Rotunno and Klemp (1985).

Since off-hodograph storm propagation is associated with environmental streamwise vorticity, the expectation is that a storm exhibiting such off-hodograph propagation is more likely to be rotational than a storm that does not exhibit off-hodograph propagation. Davies-Jones et al. (1990) proposed that a suitable measure of the tendency to produce a rotating storm could be given by integrating the magnitude of this streamwise vorticity through the depth of the primary inflow layer of the storm, h (usually taken to be 3 km):

$$H(\mathbf{c}) = -\int_0^h \mathbf{k} \cdot (\mathbf{v} - \mathbf{c}) \times \frac{d\mathbf{v}}{dz}\, dz. \tag{16}$$

This quantity, which is twice the signed area swept out by the storm-relative wind vector between the surface and 3 km on a hodograph diagram (e.g., Fig. 1) is what

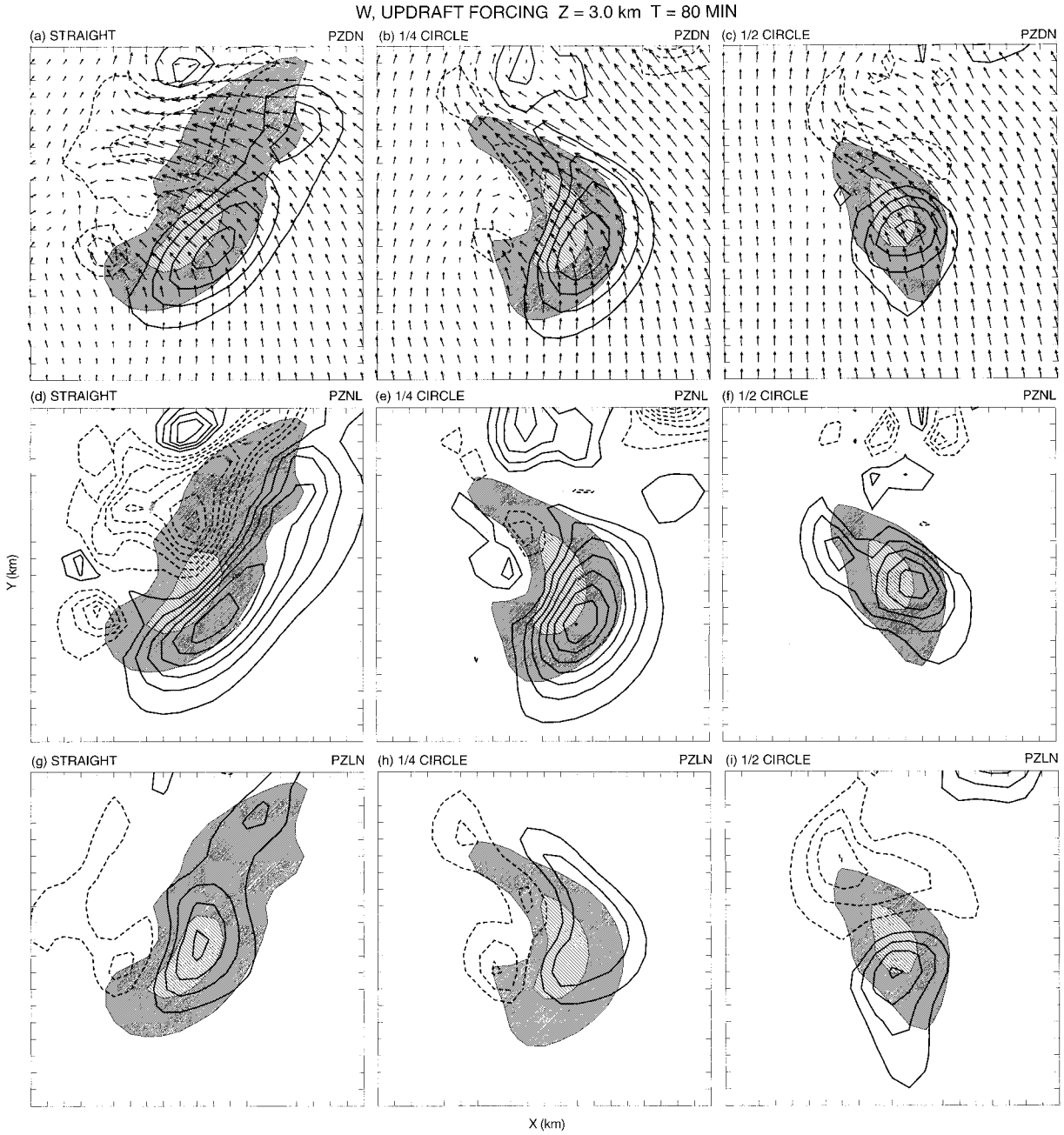

FIG. 12. Dynamic (PZDN), nonlinear (PZNL), and linear (PZLN) updraft forcing at 3 km AGL at 80 min for the (a), (d), (g) straight shear, (b), (e), (h) quarter-circle shear, and (c), (f), (i) half-circle shear simulations, respectively, as described for Fig. 10.

has come to be known as the storm-relative environmental helicity (SREH).

Given storm motion, observational and modeling studies confirm that SREH generally correctly ascertains the rotational character of supercell storms (e.g., Davies-Jones et al. 1990; Drogemeier et al. 1993; Johns et al. 1993; Brooks and Wilhelmson 1993; Brooks et al. 1994; Kerr and Darkow 1996). If one further observes that a storm generated in a strongly curved hodograph naturally exhibits a storm motion within the curve of that hodograph [based on a simple linear advection of the convective element; e.g., Davies-Jones (1984, appendix B)], then that storm would exhibit a large amount of streamwise vorticity and would, therefore, be more likely to exhibit supercell characteristics.

Indeed, the present simulations confirm that the correlation between vertical velocity and vertical vorticity increases as hodograph curvature is added to the environmental wind profile (e.g., Figs. 8 and 9). Thus, the inference could be made that supercell processes must

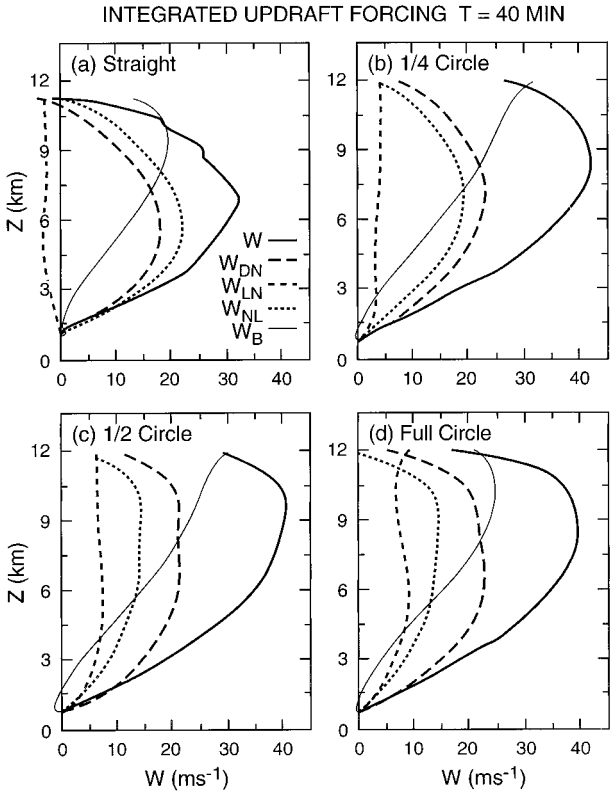

FIG. 13. Integrated contributions to updraft forcing at 40 min for the (a) straight, (b) quarter-circle, (c) half-circle, and (d) full-circle hodograph simulations. The W (thick solid line) represents the observed vertical velocity as interpolated along each trajectory, while W_{DN}, W_{LN}, W_{NL}, and W_B represent the integrated contributions to the vertical velocity along each trajectory from the dynamic, linear, nonlinear, and buoyancy terms in the vertical momentum equation, respectively, as described in the text.

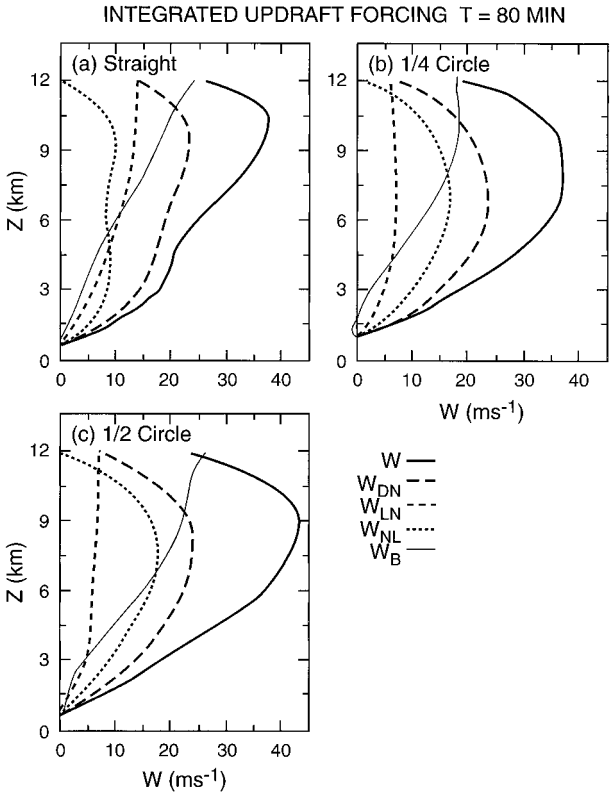

FIG. 14. Integrated contributions to updraft forcing from the dynamic, nonlinear, linear, and buoyancy terms in the vertical momentum equation at 80 min for the (a) straight, (b) quarter-circle, and (c) half-circle, as described in Fig. 13.

be essentially linear for storms developing in strongly curved hodograph settings. However, this would neglect straight-hodograph settings, wherein linear predictions of storm motion using a fully linearized model (e.g., Raymond 1975; Klemp 1987) would reside on the hodograph curve, and therefore the environmental flow would exhibit no storm-relative streamwise vorticity or SREH. Thus, the dynamics of supercells in straight-hodograph settings appear different from those in curved-hodograph settings.

Our conclusions based on the present (e.g., Figs. 10–14) and past analyses (e.g., Rotunno and Klemp 1982, 1985) emphasize that the physical mechanisms responsible for storm propagation are dominantly nonlinear for straight- and curved-shear profiles alike. For instance, we recall from Fig. 3 that the deviate propagation associated with the supercell motion develops over time (e.g., over the initial 30–60 min) as the nonlinear feedbacks are developing, also independent of hodograph curvature. Thus, assuming storm propagation, c, for the quasi-linear theories is akin to assumming the nonlinear forcing that creates the supercell in the first place. From this perspective, the quasi-linear approaches associated with SREH cannot be used to explain the existence of supercell storms. An explanation for the longevity, rotational, and propagational characteristics of supercell storms together must rely on a diagnoses of the nonlinear system of equations.

c. Beltrami solutions

A proposed advantage of emphasizing the use of strongly curved hodographs for interpreting supercell dynamics is that a circular hodograph is amenable to analytic Beltrami-type solutions, which are nonlinear and represent purely helical flows (e.g., Brooks and Wilhelmson 1993; also Lilly 1982, 1986b; Davies-Jones 1985). To obtain such solutions, we start with the momentum equation (1), with the advection term rewritten using standard vector identities:

$$\frac{\partial \mathbf{v}}{\partial t} + \boldsymbol{\nabla}\left(\frac{\mathbf{v}^2}{2}\right) - \mathbf{v} \times \boldsymbol{\omega} = -C_p \overline{\theta}_v \boldsymbol{\nabla}\pi + B\mathbf{k}. \quad (17)$$

For Beltrami solutions, the flow is assumed to be purely helical (i.e., the vorticity and velocity vectors point in the same direction), and, as such, the last term on the left-hand side of (17), often referred to as the Lamb

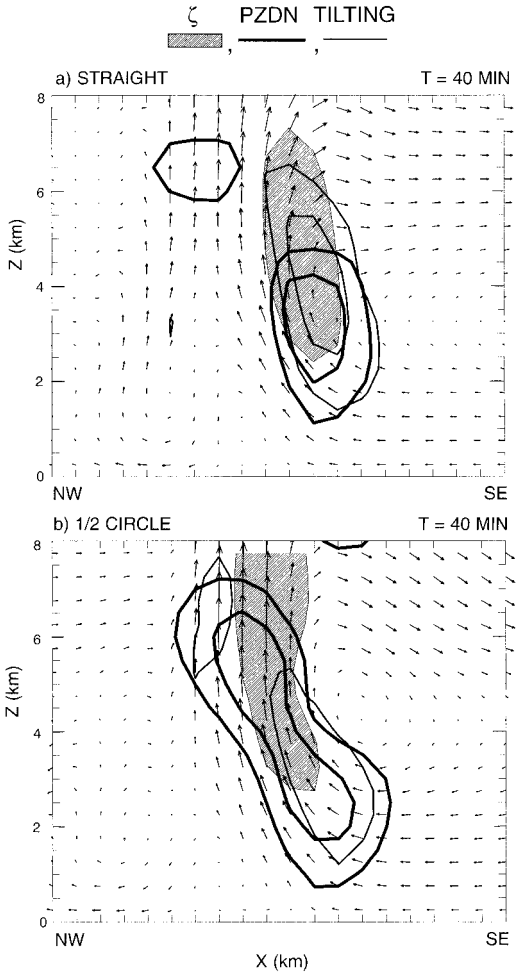

FIG. 15. Vertical cross sections of the flow field (vectors), vertical vorticity (shading), dynamic vertical pressure gradient forcing (thick contours), and tilting term (thin contours) taken northwest–southeast through the center of the right-moving updrafts for the (a) straight and (b) half-circle hodograph simulations at 40 min. Vorticity is shaded for regions greater than 0.008 s^{-1}, PZDN is contoured for 0.03 and 0.06 m s^{-2}, and the tilting term is contoured for 20 and 60 $\times$ 10^{-6} s^{-2}. A vector length of one grid interval equals a vector magnitude of 30 m s^{-1}. Tick marks are included every km in the horizontal and 500 m in the vertical.

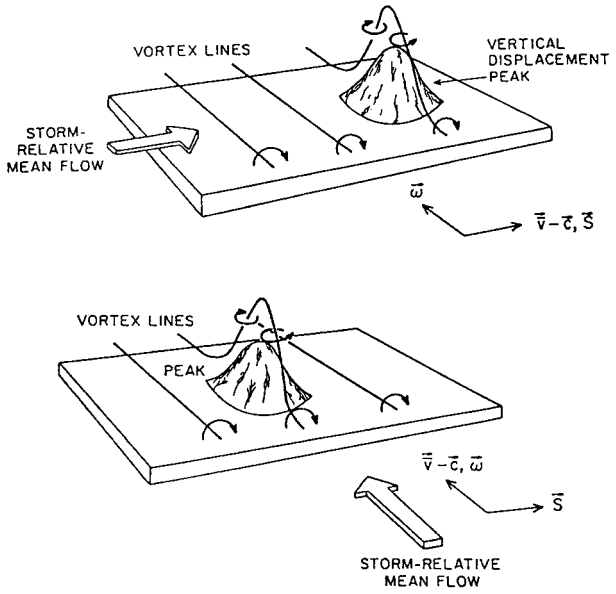

FIG. 16. Within the context of linear theory, the thunderstorm is thought of as a ''bump'' in the isentropic surface (or, more precisely, moist isentropic surface). If one gives the storm motion vector, c, then one can deduce the phase relation between vertical vorticity and vertical velocity, since the flow lines and vortex lines follow the isentropic surface. The vortex lines over the bump always imply a vertically oriented vortex pair. (top) The storm motion is purely in the shear direction, and so the updraft is collocated with the bump and so straddles (is out of phase with) the vortex pair. (bottom) The storm motion is across the shear direction, and the vertical velocity is up on the right (facing downshear) and down on the left; hence the vertical vorticity is in phase with the vertical velocity (adapted from Davies-Jones 1984).

vector, is assumed to be small (formally zero) compared to the second term on the left-hand side, which we will refer to as the Bernoulli term. Additionally, the buoyancy is set to zero, and the solution is assumed to be steady state in a reference frame moving with the storm. Solutions can be found for this system for the case of an idealized updraft propagating at the center of a circular hodograph, and estimates can be made of the dynamic updraft forcing that is consistent with such a flow configuration. As shown by Brooks and Wilhelmson (1993), this model predicts increasing dynamic updraft accelerations for increasing magnitudes of the storm-relative wind (increasing radius of the hodograph), and increasing directional shear, which seems consistent with the observed enhancement of modeled storms at early times in both the present and past studies (e.g., Droegemeier et al. 1993) for environments with strongly curved hodographs.

The question here, however, is whether this enhancement is a dominant factor in supercell dynamics. More directly, is the Beltrami solution relevant outside the special circumstances in which it might apply, and hence relevent to the full spectrum of supercell storms? To begin with, Beltrami solutions ignore buoyancy effects, which is certainly important to real supercell storms. But perhaps the more important question is whether the basic Beltrami condition of a highly helical structure holds in full supercell storms. A simple way to test this assumption is to compare the magnitudes of the Lamb vector to the magnitude of the Bernoulli term for the four simulations presented above. For this purpose, we compare the individual components of the two terms in (17) at 40 min at 3 km AGL, with the two horizontal components plotted as horizontal vectors and the vertical component contoured separately. As presented in Figs. 17 and 18, the components of the Lamb vector are found to be at least as large as the components of the Bernoulli term for all of the hodgraph shapes considered. Thus, the basic premise of the Beltrami ap-

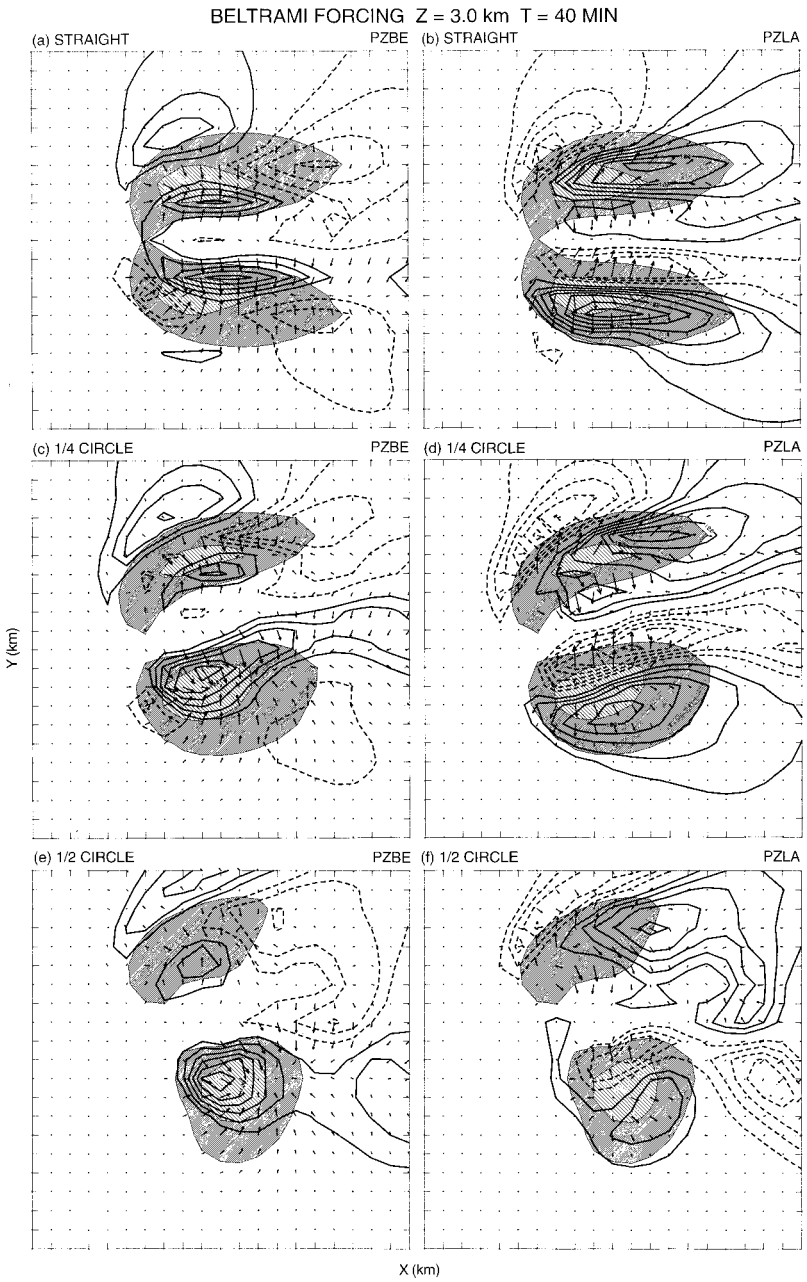

FIG. 17. Magnitude of the components of the Bernoulli and Lamb vector terms in the momentum equation at 3 km AGL at 40 min for the (a), (b) straight shear, (c), (d) quarter-circle shear, and (e), (f) half-circle shear simulations, respectively, as described in the text. The horizontal components are plotted as horizontal vectors, with a vector length of one grid interval equal to a magnitude of 0.15 m s^{-2}. The vertical component is contoured at 0.02 m s^{-2} intervals, with the zero contour ommitted. The sum of the two vertical components is essentially equivalent to the full vertical dynamic pressure gradient forcing (PZDN), as presented in Figs. 10–12. The updraft region is cross hatched, with the dark and light hatching representing vertical velocities between 4 and 14 m s^{-1}, and greater than 14 m s^{-1}, respectively. The full domain has been windowed to a 20 km by 20 km region, centered on the moving storms. Tick marks are included every km.

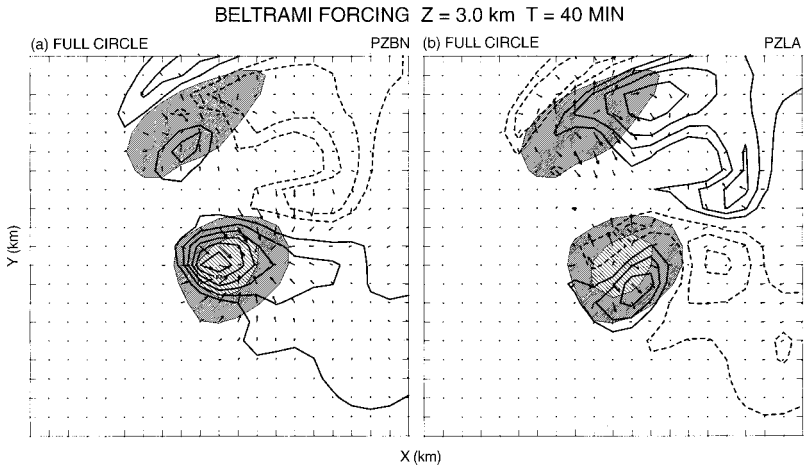

FIG. 18. Magnitude of the components of the (a) Bernoulli and (b) Lamb vector terms in the momentum equation at 3 km AGL at 40 min for the full-circle shear simulation, as described for Fig. 17.

proach, that the nonhelical contributions to the flow are insignificant, does not hold for these simulations. However, we do find that the relevance of the Beltrami solutions improves as hodograph curvature increases.

The vertical component of these terms can also be related directly to the updraft forcing, as described in section 3a, with the advective term now split into that associated with the Bernoulli effects (PZBE), and that associated with the Lamb vector, or, nonhelical effects (PZLA),

$$-C_p\overline{\theta}_v\frac{\partial\pi}{\partial z} + B = \frac{\partial(u^2/2 + v^2/2 + w^2/2)}{\partial z} - (u\omega_y - v\omega_x). \quad (18)$$

In the absence of buoyancy, the sum of the Bernoulli and Lamb contributions can be equated to the total dynamic vertical pressure gradient forcing, $-C_p\overline{\theta}_v\partial\pi_{dn}/\partial z$, as in Eq. (9). Comparing these two terms among the cases in Figs. 17 and 18, it is clear that the dynamic pressure forcing on the right flank of the storm, which we previously associated with the maintenance and propagation of the supercellular updrafts in section 3, is associated almost entirely with the vertical component of the Lamb vector, with the vertical component of the Bernoulli term contributing positively mostly on the left flank of the updraft, working counter to the observed updraft propagational tendencies. The buoyancy, *B*, is found to be collocated with the updraft (not shown). Thus, it appears as if ignoring the Lamb vector in the description of supercell dynamics is incorrect, both from the perspective of its magnitude compared to the Bernoulli term as well as its critical importance for the basic maintenance and propagation of the storm. In essence, the present results suggest that it is the specific lack of a perfect correlation between the vertical velocity and vertical vorticity field that creates the nonlinear dynamic forcing demonstrated to be critical for updraft maintenance and propagation.

4. Summary

Herein, we have attempted to compare and contrast recent theories for supercell storms through an analysis of idealized simulations of such storms for straight through fully circular-hodograph settings. The primary issue being addressed is whether the updraft–vertical wind shear theory or the streamwise vorticity–SREH theories offer the better paradigm for understanding the maintenance, propagation, and rotational characteristics of such storms. Paramount to this issue is the determination as to whether supercell processes are inherently linear or nonlinear. A directly related issue is whether the dynamics of supercell storms are inherently different for straight- versus curved-hodograph environments.

Our results reconfirm that the basic processes by which a storm develops supercell characteristics (i.e., updraft forcing, updraft rotation, storm propagation, etc.) are similar, independent of hodograph curvature. The addition of hodograph curvature, however, does enhance updraft–rotational correlations somewhat and enhances updraft strength by about 10%, especially at early times. It also enhances the development of the cyclonic right-flank storm over the anticyclonic left-flank storm, as described in previous studies. An analysis of the dynamic vertical pressure gradient term in the vertical momentum equation also reconfirms that the processes contributing to updraft maintenance and propagation are significantly nonlinear, independent of hodograph curvature. However, the linear forcing terms do provide an increasing forcing bias as hodograph curvature is added, as also previously described.

An analysis was also completed to determine whether

Beltrami solutions represent the dynamics of supercell storms for any of the hodographs considered. Our results demonstrate that the relevance of the Beltrami solutions increases for increasing hodograph curvature, but that the terms ignored in such solutions, associated with the Lamb vector, are as important as those retained for all hodograph curvatures considered.

The approach taken by the advocates of streamwise vorticity/helicity is quite distinct from the approach taken by the advocates of vertical wind shear. The vertical wind shear perspective attempts to explain the maintenance, propagation, and rotational characteristics of supercells all together. However, the maintenance and propagational characteristics are taken as a given from the helicity and Beltrami perspective and the emphasis is then placed on the processes that produce updraft rotation alone. On this issue, there is little argument. All sides agree that midlevel updraft rotation in supercell storms originates via the tilting (and subsequent stretching) of horizontal vorticity associated with the ambient shear. It is in the inferences of the streamwise vorticity–helicity perspective beyond the diagnosis of the rotational characteristics of a given storm that the disagreements begin. The essence of this debate can be summarized in terms of whether a storm generates rotation by virtue of propagation, which is the helicity–streamwise vorticity viewpoint, or whether the propagation is a result of the development of a dynamically forced, rotating updraft, which is the vertical wind shear perspective. We believe that the present results reconfirm the latter interpretation.

One of the proposed practical advantages of using the streamwise vorticity–helicity approach is that it easily characterizes supercell potential for strongly curved-hodograph settings, for which storm motion based on mean wind estimates naturally occur within the hodograph curve (leading to apparently high values of SREH). However, as noted, this viewpoint makes straight hodograph settings problematic, and, in point of fact, straight or slightly curved hodographs occur frequently in supercell scenarios, with some degree of splitting the rule rather than the exception. Indeed, the climatological hodograph most frequently associated with supercell storms (e.g., Fig. 1) is only slightly curved in the lowest layers, most closely resembling the quarter-circle shear hodograph used in the present study. As we demonstrated, the dynamics of the simulated supercell associated with this quarter-circle case was more closely aligned with the straight hodograph case than with the half-circle or full-circle shear cases. This is not surprising, since, historically, it was the observations of splitting storms that gave us the initial clues to the existence of unique supercell processes! Since the present modeling results demonstrate that the nonlinear processes inherent to splitting storms also dominate in curved hodographs, it seems more logical to accept a paradigm that includes both straight and curved hodographs rather than one that only applies to the curved-hodograph scenario.

In summary, perhaps the theory that offers the best paradigm for understanding supercell dynamics depends on the question one asks. If one is interested primarily in identifying the rotational characteristics of an observed quasi-steady, propagating storm, then the quasi-linear approaches, applied through the concept of SREH, will give a correct answer. However, if one is interested in the full time-dependent problem of what creates and maintains a rotating storm, then we believe that the updraft–shear interactions approach offers the best paradigm for understanding the full spectrum of supercell storms, independent of hodograph shape or storm propagational characteristics.

Acknowledgments. We would like to acknowledge valuable discussions and reviews of this work by Joseph Klemp, Jeffrey Trapp, Erik Rasmussen, Doug Lilly, Louis Grasso, and one anonymous reviewer.

REFERENCES

Achtemeier, G. L., 1969: Some observations of splitting thunderstorms over Iowa on August 25–26, 1965. Preprints, *Sixth Conf. on Severe Local Storms,* Chicago, IL, Amer. Meteor. Soc., 89–94.

Barnes, S. L., 1970: Some aspects of a severe, right-moving thunderstorm deduced from mesonetwork Rawindsonde observations. *J. Atmos. Sci.,* **27,** 634–678.

Bluestein, H. B., and C. J. Sohl, 1979: Some observations of a splitting severe thunderstorm. *Mon. Wea. Rev.,* **107,** 861–873.

Brooks, H. E., and R. B. Wilhelmson, 1993: Hodograph curvature and updraft intensity in numerically modeled supercells. *J. Atmos. Sci.,* **50,** 1824–1833.

——, C. A. Doswell III, and J. Cooper, 1994: On the environments of tornadic and nontornadic mesocyclones. *Wea. Forcasting,* **9,** 606–618.

Browning, K. A., 1964: Airflow and precipitation trajectories within severe local storms which travel to the right of the winds. *J. Atmos. Sci.,* **21,** 634–639.

Byers, H. R., and R. R. Braham Jr., 1949: *The Thunderstorm.* U.S. Government Printing Office, 287 pp.

Davies-Jones, R. P., 1984: Streamwise vorticity: The origin of updraft rotation in supercell storms. *J. Atmos. Sci.,* **41,** 2991–3006.

——, 1985: Dynamical interaction between an isolated convective cell and a veering environmental wind. Preprints, *14th Conf. on Severe Local Storms,* Indianapolis, IN, Amer. Meteor. Soc., 216–219.

——, and H. Brooks, 1993: Mesocyclogenesis from a theoretical perspective. *The Tornado: Its Structure, Dynamics, Prediction, and Hazards, Geophys. Monogr.,* No. 79, Amer. Geophys. Union, 105–114.

——, D. Burgess, and M. Foster, 1990: Test of helicity as a tornado forecast parameter. Preprints, *16th Conf. on Severe Local Storms,* Kananaskis, AB, Canada, Amer. Meteor. Soc., 588–592.

Droegemeier, K. K., S. M. Lazarus, and R. P. Davies-Jones, 1993: The influence of helicity on numerically simulated convective storms. *Mon. Wea. Rev.,* **121,** 2005–2029.

Fankhauser, J. C., and C. G. Mohr, 1977: Some correlations between various sounding parameters and hailstorm characteristics in northeast Colorado. Preprints, *10th Conf. on Severe Local Storms,* Omaha, NE, Amer. Meteor. Soc., 218–225.

Fujita, T., and H. Grandoso, 1968: Split of a thunderstorm into an-

ticyclonic and cyclonic storms and their motion as determined from numerical model experiments. *J. Atmos. Sci.,* **25,** 416–439.
Johns, R. H., J. M. Davies, and P. W. Leftwich, 1993: Some wind and instability parameters associated with strong and violent tornadoes. 2. Variations in the combinations of wind and instability parameters. *The Tornado: Its Structure, Dynamics, Prediction, and Hazards,* C. R. Church, Ed., Amer. Geophys. Union, 583–590.
Kanak, K. M., and D. K. Lilly, 1996: The linear stability and structure of convection in a circular mean shear. *J. Atmos. Sci.,* **53,** 2578–2593.
Kerr, B. W., and G. L. Darkow, 1996: Storm-relative winds and helicity in the tornadic thunderstorm environment. *Wea. Forecasting,* **11,** 489–505.
Klemp, J. B., 1987: Dynamics of tornadic thunderstorms. *Annu. Rev. Fluid Mech.,* **19,** 369–402.
——, and R. B. Wilhelmson, 1978a: The simulation of three-dimensional convective storm dynamics. *J. Atmos. Sci.,* **35,** 1070–1096.
——, and ——, 1978b: Simulations of right- and left-moving storms produced through storm splitting. *J. Atmos. Sci.,* **35,** 1097–1110.
——, and D. R. Durran, 1983: An upper boundary condition permitting internal gravity wave radiation in numerical mesoscale models. *Mon. Wea. Rev.,* **111,** 430–444.
Lemon, L. R., and C. A. Doswell III, 1979: Severe thunderstorm evolution and mesocyclone structure as related to tornadogenesis. *Mon. Wea. Rev.,* **107,** 1184–1197.
Lilly, D. K., 1979: The dynamical structure and evolution of thunderstorms and squall lines. *Annu. Rev. Earth Planet. Sci.,* **7,** 117–161.
——, 1982: The development and maintenance of rotation in convective storms. *Intense Atmospheric Vortices,* L. Bengtsson and J. Lighthill, Eds., Springer-Verlag, 149–160.
——, 1986a: The structure, energetics and propagation of rotating convective storms. Part I: Energy exchange with the mean flow. *J. Atmos. Sci.,* **43,** 113–125.
——, 1986b: The structure, energetics and propagation of rotating convective storms. Part II: Helicity and storm stabilization. *J. Atmos. Sci.,* **43,** 126–140.
Maddox, R. A., 1976: An evaluation of tornado proximity wind and stability data. *Mon. Wea. Rev.,* **104,** 133–142.
McCaul, E. W., Jr., and M. L. Weisman, 1996: Simulations of shallow supercell storms in landfalling hurricane environments. *Mon. Wea. Rev.,* **124,** 408–429.
Newton, C. W., and H. R. Newton, 1959: Dynamical interactions between large convective clouds and environments with vertical shear. *J. Meteor.,* **16,** 483–496.
Ogura, Y., and N. A. Phillips, 1962: Scale analysis of deep and shallow convection in the atmosphere. *J. Atmos. Sci.,* **19,** 173–179.
Panofsky, H. A., and G. W. Brier, 1968: *Some Application of Statistics to Meteorology.* The Pennsylvania State University, 224 pp.
Raymond, D. J., 1975: A model for predicting the movement of continuously propagating convective storms. *J. Atmos. Sci.,* **32,** 1308–1317.
Rotunno, R., 1981: On the evolution of thunderstorm rotation. *Mon. Wea. Rev.,* **109,** 577–586.
——, and J. B. Klemp, 1982: The influence of the shear-induced pressure gradient on thunderstorm motion. *Mon. Wea. Rev.,* **110,** 136–151.
——, and ——, 1985: On the rotation and propagation of simulated supercell thunderstorms. *J. Atmos. Sci.,* **42,** 271–292.
Schlesinger, R. E., 1980: A three-dimensional numerical model of an isolated thunderstorm. Part II: Dynamics of updraft splitting and mesovortex couplet evolution. *J. Atmos. Sci.,* **37,** 395–420.
Weisman, M. L., and J. B. Klemp, 1982: The dependence of numerically simulated convective storms on vertical wind shear and buoyancy. *Mon. Wea. Rev.,* **110,** 504–520.
——, and ——, 1984: The structure and classification of numerically simulated convective storms in directionally varying wind shears. *Mon. Wea. Rev.,* **112,** 2479–2498.
——, and ——, 1986: Characteristics of isolated convective storms. *Mesoscale Meteorology and Forecasting,* P. S. Ray, Ed., Amer. Meteor. Soc., 331–358.